

## COMMUNICATION

# Chromophore-assisted proximity labeling of DNA reveals chromosomal organization in living cells

Tao Ding<sup>1,#</sup>, Liyuan Zhu<sup>1,#</sup>, Yuxin Fang<sup>1</sup>, Yangluorong Liu<sup>1</sup>, Wei Tang<sup>2,3</sup>, Peng Zou<sup>1,3,4,5,\*</sup>Dedicated to the 100<sup>th</sup> Birthday of Professor Youqi Tang

1. College of Chemistry and Molecular Engineering, Synthetic and Functional Biomolecules Center, Beijing National Laboratory for Molecular Sciences, Key Laboratory of Bioorganic Chemistry and Molecular Engineering of Ministry of Education, Peking University, Beijing, 100871, China
2. Academy for Advanced Interdisciplinary Studies, Peking University, Beijing, 100871, China
3. Peking-Tsinghua Center for Life Sciences, Beijing, 100871, China
4. PKU-IDG/McGovern Institute for Brain Research, Beijing, 100871, China
5. Chinese Institute for Brain Research (CIBR), Beijing 102206, China

\* Correspondence: [zoupeng@pku.edu.cn](mailto:zoupeng@pku.edu.cn)

# These authors contributed equally to this work.

**Abstract:** The spatial arrangement of chromosome within the nucleus is intimately linked to genome function and gene expression regulation. Existing genome-wide mapping methods to study chromosome organization often rely on chemically crosslinking DNA with protein baits, which raises concerns of introducing artifacts during cellular fixation. Herein, we developed a novel proximity-dependent DNA labeling method based on the chromophore-assisted nucleobase photooxidation. By genetically targeting a photosensitizer protein to specific subnuclear locations, we achieved blue light-activated labeling of local DNA with a bioorthogonal functional handle, which allowed subsequent affinity purification and sequence identification via next-generation sequencing. When applied to the nuclear lamina in human embryonic kidney 293T cells, our method revealed lamina-associated domains (LADs) that cover 37.6% of the genome. These LADs overlap with heterochromatin hallmarks including histone 3 lysine 9 dimethylation (H3K9me2) and are depleted with CpG islands. This simple labeling method avoids the harsh treatment of chemical crosslinking and is generally applicable to the genome-wide high-resolution mapping of the spatial chromosome organization in living cells.

In eukaryotic cells, the three-dimensional chromosome architecture has profound effects on gene functions<sup>[1-2]</sup>. The formation of local chromatin structures is crucially involved in a diverse array of biological processes, ranging from gene activation<sup>[3-4]</sup> to replication timing<sup>[5-6]</sup>. For example, genomic regions associated with the nuclear lamina, a fibrillar network at the periphery of the nucleus, are mainly composed of silent genes. Moreover, dysregulated chromatin structures have been implicated in many diseases<sup>[7]</sup>, and manipulation of 3D genome has been shown to alter gene expression levels and cellular functions<sup>[8-9]</sup>.

Conventional approaches for studying DNA-protein interactions and the spatial arrangement of chromatin, such as chromatin immunoprecipitation-sequencing (ChIP-seq), often require formaldehyde-mediated chemical crosslinking, which may introduce bias<sup>[10]</sup>. In addition, successful immunoprecipitation depends critically on the availability of specific antibodies against the bait protein. Alternatively, various proximity labeling techniques have been developed to profile DNA-protein contacts at specific subcellular locations. For example, by employing enzyme-mediated DNA methylation near a bait protein, DamID (DNA adenine methyltransferase identification) has been widely

used to investigate protein-DNA interactions *in vivo*<sup>[11-12]</sup>. Recently, an antibody-targeted peroxidase-mediated labeling strategy, termed TSA-seq, was developed to biotinylate proximal DNA with phenoxy free radicals, which has revealed chromatin organization near the nuclear lamina and nuclear speckle in fixed cells<sup>[13]</sup>. Each of these methods has its own merits and weaknesses. For example, TSA-seq requires cellular fixation and membrane permeabilization to allow the intracellular delivery of antibody-peroxidase conjugate, while DamID-catalyzed DNA methylation is restricted to labeling adenine within the palindromic tetrad sequence GATC<sup>[11]</sup>.

Herein, we present a conceptually novel DNA proximity labeling technique that offers both high spatial and high temporal resolutions in live cells. Our method is built upon the photosensitized DNA oxidative damage. Among all four DNA nucleobases, guanine has the lowest redox potential and is readily oxidized by singlet oxygen (<sup>1</sup>O<sub>2</sub>) to yield a range of products, including spiroiminodihydroantoin (Sp), imidazolone (Iz), oxazolone (Oz), etc.<sup>[14]</sup> We chose miniSOG, an engineered flavoprotein originally derived from *A. thaliana* phototropin 2, as the photosensitizer because it can be genetically targeted to specific subnuclear locations in the form of protein fusion<sup>[15]</sup>. Upon blue light illumination, miniSOG generates <sup>1</sup>O<sub>2</sub> via type II photoreaction<sup>[16]</sup>.

While this chromophore-assisted proximity labeling strategy has been previously implemented by our group and others to profile the spatial organization of RNA<sup>[17-19]</sup>, it cannot be easily extended to labeling DNA because of the following unique challenges associated with chromatin: 1) substantially lower copy number of DNA (2 in diploid cells) compared to RNA (often >100 per cell); 2) lower reactivity of double-stranded DNA (dsDNA) versus single-stranded RNA<sup>[17]</sup>; and 3) shielding of DNA by nucleosome and higher order chromatin structures. These challenges have necessitated improvements in both chemical labeling and analytical methods.

We started with characterizing miniSOG-mediated DNA photooxidation *in vitro*. In a mixture of 100 μM miniSOG and 2.5 mM guanosine in aqueous solution, blue light illumination at the modest intensity of 24 mW/cm<sup>2</sup> caused a gradual consumption of the guanosine starting material, with a half-life of approximately 35 min, as monitored by the ultra-high performance liquid chromatography-mass spectrometry (UPLC-MS) (Fig. 1A-B and Fig. S1). Meanwhile, more polar oxidation products were formed

## COMMUNICATION

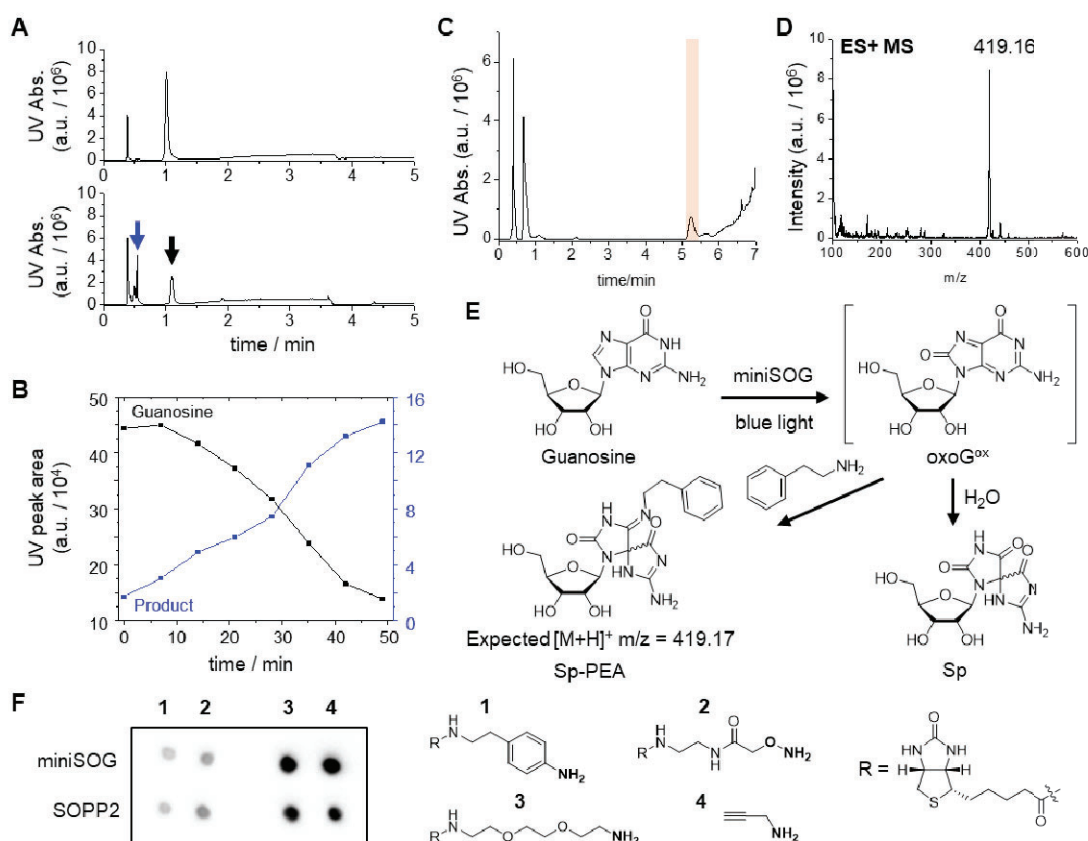


**Figure 1. Characterization of miniSOG/SOPP2-mediated DNA labeling.** (A) UPLC analysis of miniSOG-mediated guanosine oxidation before (top) and after (bottom) blue light illumination for 49 min. Black and blue arrows point to guanosine and its oxidation products, respectively. The peak observed at 0.4 min corresponds to buffer components that elute at the dead volume. (B) The progress of miniSOG-mediated guanosine oxidation reaction, as monitored by UPLC at various illumination intervals. (C) UPLC-MS analysis of miniSOG-mediated guanosine oxidation and phenethylamine (PEA) adducts formation, with an elution gradient different from those applied in (A) (see [Supplementary Method](#)). (D) ES+ MS analysis of the shaded area in (C). (E) Proposed reaction scheme of photo-oxidative conjugation between guanosine and PEA via the intermediate of oxoG<sup>ox</sup>. Whereas oxoG<sup>ox</sup> hydrolysis leads to the formation of Sp, it could react with PEA to form the adduct Sp-PEA, whose *m/z* matches the result of ES+ MS analysis in (D). (F) Streptavidin-HRP dot blot analysis of miniSOG/SOPP2-mediated DNA labeling with various biotin-conjugated amine probes. For propargyl amine (PA, 4), click reaction with N<sub>3</sub>-biotin is performed after light illumination. The right panel shows the chemical structure of amine probes used in this study.

(less retention time on the reverse-phase column), with *m/z* values matching those of Iz, Sp, and Oz (Fig. S2). With the knowledge that guanosine could be oxidatively conjugated to amine-functionalized molecules such as lysine and spermine<sup>[20-21]</sup>, we repeated the above photooxidation experiment with 10 mM phenethylamine (PEA) added to the reaction mixture. As expected, we detected a new product with *m/z* matching that of the oxidative conjugate, Sp-PEA (Fig. 1C-E and Fig. S3). Another engineered flavoprotein SOPP2, which is a mutant of miniSOG with improved <sup>1</sup>O<sub>2</sub> quantum yield<sup>[22]</sup>, could also mediate the formation of Sp-PEA adduct (Fig. S3).

We further exploited the above photooxidation reaction to covalently attach biotin to dsDNA. Firstly, using dot blot assay as a readout for biotinylation, we compared several biotin-conjugated amine probes, including aniline (1), alkoxylamine (2), and alkyl amine (3) (Fig. 1F). Among these, alkyl amine (3) exhibited the highest reactivity towards miniSOG-mediated photo labeling of dsDNA. SOPP2-mediated labeling yielded similar biotinylation signal as miniSOG. Secondly, we confirmed that the biotinylation is dependent on both the presence of miniSOG and blue light illumination (Fig. S4). Thirdly, using enzymatic digestion assays, we excluded the possibility of miniSOG self-labeling as the major source of the observed biotinylation signal on the dot blot. When the labeled sample was treated with DNase I, we

noticed a substantial decrease in the dot blot signal, whereas treatment with RNase A or proteinase K caused little changes (Fig. S4). Finally, when the biotin moiety was replaced with a bioorthogonal functional handle such as an alkyne, the resulting propargyl amine (PA, 4) probe could also be photooxidatively conjugated to dsDNA and subsequently derivatized with biotin using Cu-assisted alkyne-azide cycloaddition (CuAAC) reaction (Fig. 1F and [Supplementary Method](#)). Taken together, these data demonstrated that miniSOG could mediate the photooxidative conjugation of amine probes to dsDNA upon blue light illumination.

We next sought to test the efficiency and the spatial specificity of chromophore-assisted dsDNA labeling in the cellular context. Through fusions with the *N*-terminal signal sequence of COX4 (mito-miniSOG), histone 2B (H2B-miniSOG/SOPP2), lamin A (SOPP2-LMNA), and nucleolin (SOPP2-NCL), miniSOG/SOPP2 was targeted to the mitochondrial matrix, the nucleoplasm, the nuclear lamina, and the nucleolus, respectively, in human embryonic kidney 293T (HEK293T) cells (Fig. 2A and Fig. S5). For intracellular labeling, we chose PA (4) as the probe for its excellent water solubility and cell membrane permeability<sup>[17]</sup>. Following probe incubation (5 mM) at 37°C for 10 min, cells expressing mito-miniSOG and H2B-miniSOG were illuminated with blue light at 28 mW/cm<sup>2</sup> for 15 min. Immunofluorescence

## COMMUNICATION

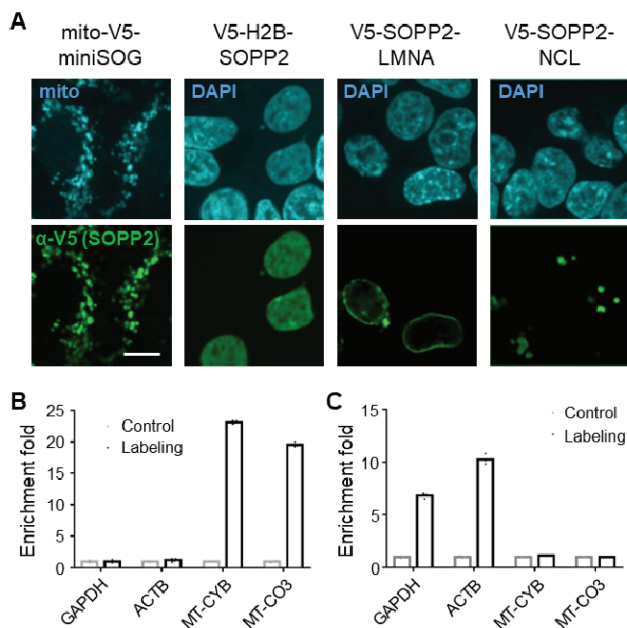


**Figure 2. Characterization of the efficiency and the spatial specificity of miniSOG/SOPP2-mediated DNA labeling in the cellular context.** (A) Immunofluorescence images of HEK293T cells expressing mito-miniSOG, H2B-SOPP2, SOPP2-LMNA, and SOPP2-NCL. V5 is an epitope tag (green). Mitotracker and DAPI (cyan) are markers for the mitochondria and the nucleus, respectively. miniSOG/SOPP2 fusion proteins are expressed in a fraction of cells. Scale bar is 10  $\mu$ m. (B-C) qPCR analysis of DNA labeling in the mitochondrial matrix (B, mito-miniSOG) or the nucleoplasm (C, H2B-SOPP2).

imaging showed that no labeling occurred in cells not expressing miniSOG (Fig. S5). Thereafter, cells were lysed to extract the genomic DNA, and a biotin handle was introduced via click reaction, which allowed efficient affinity purification of labeled dsDNA fragments with streptavidin-coated beads. Finally, these enriched fragments were analyzed by quantitative PCR (qPCR) to evaluate the level of enrichment (Supplementary Method).

As expected, for DNA samples from cells expressing mito-miniSOG, mitochondrial genome-encoded genes MT-CO3 and MT-CYB showed high levels of enrichment ( $19.49 \pm 0.48$  and  $23.12 \pm 0.30$ ), whereas nuclear genome-encoded genes GAPDH and ACTB showed no enrichment relative to the control ( $1.02 \pm 0.26$  and  $1.23 \pm 0.31$ ) (Fig. 2B). The opposite was observed in DNA samples from cells expressing H2B-miniSOG: high-level enrichment of GAPDH ( $2.68 \pm 0.46$ ) and ACTB ( $2.44 \pm 1.07$ ) and no enrichment of MT-CO3 ( $1.00 \pm 0.07$ ) and MT-CYB ( $0.67 \pm 0.33$ ) (Fig. S5). By replacing H2B-miniSOG with H2B-SOPP2, much higher levels of enrichment for nuclear genes ( $6.80 \pm 0.29$  for GAPDH and  $10.26 \pm 0.54$  for ACTB) were achieved (Fig. 2C), presumably due to the higher  $^1\text{O}_2$  quantum yield of SOPP2. It is possible that the lower copy number of DNA relative to RNA calls for more intense labeling reaction to raise the signal above the noise<sup>[17]</sup>. Consistent with this observation, H2B-SOPP2 also yielded stronger biotinylation signal than H2B-miniSOG on dot blot analysis (Fig. S6). We thus decided to use SOPP2 instead of miniSOG for subsequent cellular experiments.

We then focused our analysis on the next-generation sequencing (NGS) of DNA samples. As expected, for cells expressing mito-miniSOG, NGS reads are highly enriched across the entire mitochondrial chromosome (ChrM), whereas for cells expressing H2B-SOPP2, ChrM reads were significantly depleted (Fig. S7). When SOPP2 was targeted to the nucleus via fusion

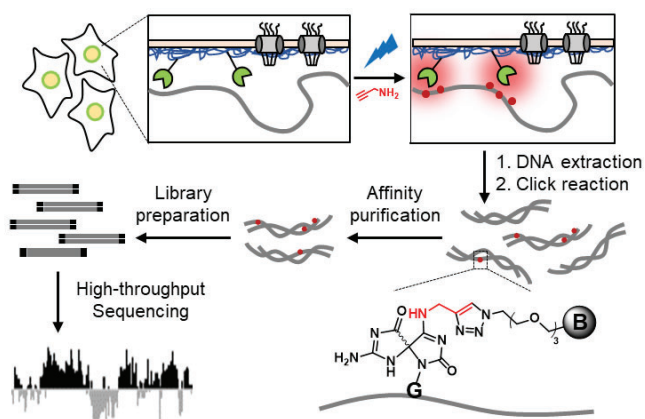


**Figure 3. Schematic of DNA labeling in HEK293T cells expressing SOPP2-LMNA.** Cells were incubated with 5 mM PA probe (4) for 10 min at 37°C before blue light illumination. Following labeling, the genome was extracted from cells and the biotin handle (grey blob) was introduced via click reaction. Finally, labeled DNA was enriched with streptavidin beads and analyzed by NGS sequencing.

with a nuclear localization sequence (SOPP2-NLS), our NGS analysis revealed a positive yet modest correlation (Pearson's correlation coefficient  $r = 0.29$ ) between SOPP2-mediated DNA enrichment and DNA single-strandness, which was measured by the level of enrichment in kethoxal-assisted single-stranded DNA sequencing (KAS-seq)<sup>[23]</sup> (Fig. S8). While this observation is consistent with the previous report that photosensitized reaction favors ssDNA over dsDNA<sup>[17]</sup>, the weak correlation between our SOPP2-NLS dataset and KAS-seq suggests that this selection rule is not stringent. Together, the above data confirmed the efficiency and high spatial specificity of chromophore-assisted DNA labeling in live cells.

Finally, we applied our method to profile local genomic sequences at the nuclear periphery. Previous DamID studies have identified chromosomal regions in close contact with the nuclear lamina. These lamina-associated domains (LADs) serve to organize chromosomes within the nucleus and have been associated with gene repression<sup>[24]</sup>. We performed two biological replicate experiments in HEK293T cells expressing SOPP2-LMNA (Fig. 2A). Following labeling and affinity purification, we analyzed enriched DNA fragments with NGS (Fig. 3).

The genomic map of enrichment was generated by plotting the  $\log_2$  ratios of enriched reads versus input reads for both replicates (Fig. 4A). To assign LADs and inter-LADs (iLADs) regions, we applied a two-state hidden Markov model (HMM)<sup>[25]</sup> for our replicated data. The LADs identified by SOPP2-LMNA cover 37.6% of the genome (Fig. S9) and have a lower gene density (3.9 genes/Mb) than iLADs (9.8 genes/Mb). For comparison, the average gene density across the whole genome is 7.4 genes/Mb. Our data thus revealed the gene-poor nature of LADs, which is consistent with the previous report<sup>[26]</sup>. Interestingly, these LADs are negatively and weakly correlated with ssDNA peaks identified by KAS-seq<sup>[23]</sup> (Fig. S10), suggesting that the weak preference of SOPP2-mediated labeling towards ssDNA is outweighed by its proximity effect.

LADs identified in our study are enriched in the heterochromatin marker H3K9me2 while depleted in histone markers associated with active gene expression, including H3K27ac, H3K4me3 and H3K36me3<sup>[27]</sup> (Fig. 4B). Certain types of repetitive elements have been associated with

## COMMUNICATION

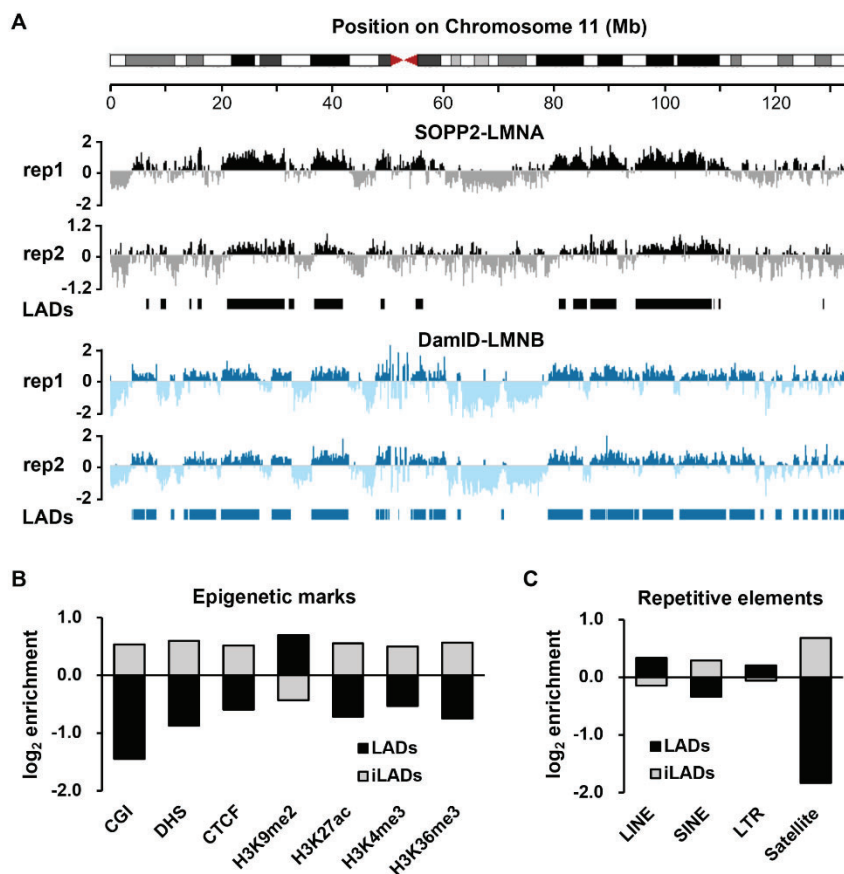


**Figure 4. Analysis of SOPP2-LMNA labeling.** (A) Integrated Genomics Viewer (IGV) browser views of DNA profiling ( $\log_2$  enrich/input) with SOPP2-LMNA replicates and DamID-LMNB in chromosome 11. (B) Epigenetic marker enrichment in LADs profiled by SOPP2-LMNA. CGI, CpG islands. DHS, DNA highly sensitive sites. (C) Relative enrichment of major repetitive elements in LADs profiled by SOPP2-LMNA. DNase-seq, CTCF ChIP-seq, and histone modifications data are from ENCODE (DNase-seq: ENCFF127KSH, CTCF: ENCFF008LSM, H3K9me2: ENCFF823KJS, H3K27ac: ENCFF993MZN, H3K4me3: ENCFF498ERO, H3K36me3: ENCFF111DMJ). Information on CGI and repetitive elements are from UCSC genome browser.

heterochromatin<sup>[25]</sup>. In our dataset, transposable elements including long interspersed nuclear elements (LINEs) and long-terminal repeats (LTRs) are enriched, while short interspersed nuclear elements (SINEs) and satellite repeats are depleted (Fig. 4C).

As expected, our SOPP2-LMNA dataset correlates well with the previous LMNA ChIP-seq data from HeLa cells<sup>[28]</sup>, but poorly with H2B-SOPP2 dataset ( $r < 0.15$ ), where the entire genome is labeled indiscriminately (Fig. S11). Furthermore, our SOPP2-LMNA dataset shares 77.5% overlap with LADs identified in previous DamID studies (Fig. 4A and Fig. S12), despite differences in cell lines (Tig3 versus HEK293T) and nuclear lamina marker protein fusions (LMNB versus LMNA) used in these experiments<sup>[26]</sup>. The above comparison highlights the conserved organization of LADs and demonstrates the power of our method in profiling DNA within subnuclear structures.

To summarize, we developed a novel method to study the spatial arrangement of chromatin in living cells. We demonstrated that genetically encoded photosensitizers, miniSOG and SOPP2, could mediate the photooxidative conjugation of amine probes to double-stranded DNA under mild blue light illumination. We applied the chromophore-assisted DNA labeling method to investigate the local chromatin sequence at the nuclear lamina and identified lamina-associated domains (LADs) that share similar features with those obtained from previous ChIP-seq and

DamID studies, thus highlighting the high spatial resolution of our new method.

Compared to existing techniques for profiling DNA sequences associated with certain subnuclear structures, such as ChIP-seq and the more recently developed TSA-seq, a notable advantage of our method is the avoidance of chemical fixatives, such that DNA labeling occurs when all the subcellular structures are preserved in their native state. In terms of substrate preference, DamID requires the presence of the GATC tetrad sequence, while photooxidative DNA damage only requires the presence of guanosine. Thus, our method could complement DamID for the high-resolution mapping of local DNA contents in live cells. Another advantage of our method is its fast reaction kinetics, requiring only 15-min illumination of blue light at modest intensities of 20-30 mW/cm<sup>2</sup>. This high temporal resolution compares favorably to DamID, which typically requires several hours of labeling<sup>[12]</sup>, and could enable future investigations of chromatin structure through different phases of the cell cycle.

Notably, chromophore-assisted proximity labeling has been previously employed for studying the spatial arrangement of subcellular transcriptome<sup>[17-19]</sup>, but has never been developed in the context of mapping chromosome organization. The size of SOPP2 (12 kDa) is less than half of those of GFP (27 kDa) and DamID (32 kDa). Given the already successful applications of GFP- and DamID-fusions in many subnuclear compartments (e.g. nucleolus<sup>[29]</sup>, nuclear speckle<sup>[30]</sup>, PML body<sup>[31]</sup>, polycomb body<sup>[32]</sup>

## COMMUNICATION

etc.), we envision that chromophore-assisted DNA labeling could be broadly applied to profile chromatin compositions in nuclear bodies and subnuclear liquid condensates that underlie transcriptional control<sup>[33]</sup>.

## Acknowledgements

We thank Y. Zhou for assistance with chemical synthesis, X. Chen (Peking University) for providing miniSOG plasmid, and P. Wang, Y. Zhou, G. Wang for helpful discussions. This work was supported by the Ministry of Science and Technology (2018YFA0507600, 2017YFA0503600), the National Natural Science Foundation of China (91753131, 21727806), and the National Science Foundation of Beijing Municipality (5182011). PZ is sponsored by Li Ge-Zhao Ning Life Science Junior Research Fellowship and Bayer Investigator Award. The authors thank the National Center for Protein Sciences at Peking University in Beijing, China, for assistance with Fragment Analyzer 12.

**Keywords:** photooxidation • DNA • proximity labeling • miniSOG

- [1] B. Bonev, G. Cavalli, *Nat Rev Genet* **2016**, *17*, 661-678.
- [2] J. Dekker, A. S. Belmont, M. Guttman, V. O. Leshyk, J. T. Lis, S. Lomvardas, L. A. Mirny, C. C. OShea, P. J. Park, B. Ren, J. C. R. Politz, J. Shendure, S. Zhong, D. N. Network, *Nature* **2017**, *549*, 219-226.
- [3] M. C. Driscoll, C. S. Dobkin, B. P. Alter, *Proc Natl Acad Sci U S A* **1989**, *86*, 7470.
- [4] L. Guelen, L. Pagie, E. Brasset, W. Meuleman, M. B. Faza, W. Talhout, B. H. Eussen, A. de Klein, L. Wessels, W. de Laat, B. van Steensel, *Nature* **2008**, *453*, 948-951.
- [5] B. D. Pope, T. Ryba, V. Dileep, F. Yue, W. Wu, O. Denas, D. L. Vera, Y. Wang, R. S. Hansen, T. K. Canfield, R. E. Thurman, Y. Cheng, G. Gulsoy, J. H. Dennis, M. P. Snyder, J. A. Stamatoyannopoulos, J. Taylor, R. C. Hardison, T. Kahveci, B. Ren, D. M. Gilbert, *Nature* **2014**, *515*, 402-405.
- [6] J. Sima, A. Chakraborty, V. Dileep, M. Michalski, K. N. Klein, N. P. Holcomb, J. L. Turner, M. T. Paulsen, J. C. Rivera-Mulia, C. Trevilla-Garcia, D. A. Bartlett, P. A. Zhao, B. K. Washburn, E. P. Nora, K. Kraft, S. Mundlos, B. G. Bruneau, M. Ljungman, P. Fraser, F. Ay, D. M. Gilbert, *Cell* **2019**, *176*, 816-830 e818.
- [7] M. T. Maurano, R. Humbert, E. Rynes, R. E. Thurman, E. Haugen, H. Wang, A. P. Reynolds, R. Sandstrom, H. Qu, J. Brody, A. Shafer, F. Neri, K. Lee, T. Kuttyavin, S. Stehling-Sun, A. K. Johnson, T. K. Canfield, E. Giste, M. Diegel, D. Bates, R. S. Hansen, S. Neph, P. J. Sabo, S. Heimfeld, A. Raubitschek, S. Ziegler, C. Cotsapas, N. Sotoodehnia, I. Glass, S. R. Sunyaev, R. Kaul, J. A. Stamatoyannopoulos, *Science* **2012**, *337*, 1190-1195.
- [8] A. Gonzalez-Sandoval, B. D. Towbin, V. Kalck, D. S. Cabianca, D. Gaidatzis, M. H. Hauer, L. Geng, L. Wang, T. Yang, X. Wang, K. Zhao, S. M. Gasser, *Cell* **2015**, *163*, 1333-1347.
- [9] H. Wang, X. Xu, C. M. Nguyen, Y. Liu, Y. Gao, X. Lin, T. Daley, N. H. Kipniss, M. La Russa, L. S. Qi, *Cell* **2018**, *175*, 1405-1417 e1414.
- [10] A. Gavrilov, S. V. Razin, G. Cavalli, *Brief Funct Genomics* **2015**, *14*, 163-165.
- [11] B. van Steensel, S. Henikoff, *Nat Biotechnol.* **2000**, *18*, 424-428.
- [12] G. N. Aughey, T. D. Southall, *Wiley Interdiscip Rev Dev Biol* **2016**, *5*, 25-37.
- [13] Y. Chen, Y. Zhang, Y. Wang, L. Zhang, E. K. Brinkman, S. A. Adam, R. Goldman, B. van Steensel, J. Ma, A. S. Belmont, *J Cell Biol* **2018**, *217*, 4025-4048.
- [14] K. Kino, M. Hirao-Suzuki, M. Morikawa, A. Sakaga, H. Miyazawa, *Genes and Environ* **2017**, *39*.
- [15] X. Shu, V. Lev-Ram, T. J. Deerinck, Y. Qi, E. B. Ramko, M. W. Davidson, Y. Jin, M. H. Ellisman, R. Y. Tsien, *PLoS Biol* **2011**, *9*, e1001041.
- [16] R. Ruiz-Gonzalez, A. L. Cortajarena, S. H. Mejias, M. Agut, S. Nonell, C. Flors, *J Am Chem Soc.* **2013**, *135*, 9564-9567.
- [17] P. Wang, W. Tang, Z. Li, Z. Zou, Y. Zhou, R. Li, T. Xiong, J. Wang, P. Zou, *Nat Chem Biol* **2019**, *15*, 1110-1119.
- [18] Y. Li, M. B. Aggarwal, K. Ke, K. Nguyen, R. C. Spitale, *Biochemistry-US* **2018**, *57*, 1577-1581.
- [19] Y. Li, M. B. Aggarwal, K. Nguyen, K. Ke, R. C. Spitale, *ACS Chem Biol.* **2017**, *12*, 2709-2714.
- [20] M. E. Hosford, J. G. Muller, C. J. Burrows, *J Am Chem Soc.* **2004**, *126*, 9540-9541.
- [21] X. Xu, J. G. Muller, Y. Ye, C. J. Burrows, *J Am Chem Soc.* **2008**, *130*, 703-709.
- [22] M. Westberg, M. Bregnhøj, M. Etzerodt, P. R. Ogilby, *J Phys Chem B* **2017**, *121*, 9366-9371.
- [23] T. Wu, R. Lyu, Q. You, C. He, *Nat Methods* **2020**, *17*, 515-523.
- [24] B. van Steensel, A. S. Belmont, *Cell* **2017**, *169*, 780-791.
- [25] W. Meuleman, D. Peric-Hupkes, J. Kind, J. B. Beaudry, L. Pagie, M. Kellis, M. Reinders, L. Wessels, B. van Steensel, *Genome Res* **2013**, *23*, 270-280.
- [26] C. Lenain, C. A. de Graaf, L. Pagie, N. L. Visser, M. de Haas, S. S. de Vries, D. Peric-Hupkes, B. van Steensel, D. S. Peeper, *Genome Res* **2017**, *27*, 1634-1644.
- [27] A. J. Bannister, T. Kouzarides, *Cell Res* **2011**, *21*, 381-395.
- [28] E. G. Lund, I. Duband-Goulet, A. Oldenburg, B. Buendia, P. Collas, *Nucleus* **2015**, *6*, 30-39.
- [29] D. Y. Chen, S. Huang, *Journal of Cell Biology* **2001**, *153*, 169-176.
- [30] K. Tripathi, V. K. Parnaik, *J Biosciences* **2008**, *33*, 345-354.
- [31] P. Brand, T. Lenser, P. Hemmerich, *PMC Biophys* **2010**, *3*, 3.
- [32] B. Tolhuis, I. Muijers, E. de Wit, H. Teunissen, W. Talhout, B. van Steensel, M. van Lohuizen, *Nature Genetics* **2006**, *38*, 694-699.
- [33] B. R. Sabari, A. Dall'Agnesse, A. Boija, I. A. Klein, E. L. Coffey, K. Shrinivas, B. J. Abraham, N. M. Hannett, A. V. Zamudio, J. C. Manteiga, C. H. Li, Y. E. Guo, D. S. Day, J. Schuijers, E. Vasile, S. Malik, D. Hnisz, T. I. Lee, I. I. Cisse, R. G. Roeder, P. A. Sharp, A. K. Chakraborty, R. A. Young, *Science* **2018**, *361*.